Int. J. Heat Mass Transfer. Vol. 19, pp. 1161–1172. Pergamon Press 1976. Printed in Great Britain

PREDICTIONS OF TWO-DIMENSIONAL BOUNDARY LAYERS ON SMOOTH WALLS WITH A TWO-EQUATION MODEL OF TURBULENCE

K. H. NG and D. B. SPALDING
Imperial College of Science and Technology, Department of Mechanical Engineering, Exhibition Road, London S.W.7.

(*Received* 16 *February* 1976)

Abstract—Two-dimensional, steady, incompressible, turbulent, hydrodynamic boundary layers near walls have been calculated with the aid of a model of turbulence relating the turbulent shear stress to the product of: the square root of local energy of turbulence, a length-scale of turbulence and the gradient time-mean velocity. Both the length scale and the energy are calculated from parabolic differential equations, solved simultaneously with that for momentum. Boundary layers exhibiting a large variety of streamwise pressure distributions, viz. those featured in the 1968 Stanford Conference, have been successfully predicted. Methods of extension to heat-transfer prediction are discussed.

NOMENCLATURE

a, b, c, d, constants;
C_D, constant;
C_P, C_M, C_W, constants;
E, constants;
e, $\equiv \frac{1}{2}(\overline{u_1^2} + \overline{u_2^2} + \overline{u_3^2})$, turbulent kinetic energy;
H_{12}, $\equiv \delta_1/\delta_2$, shape factor;
l, length scale of turbulence;
l_m, mixing-length;
P, mean pressure in free stream;
q, constant;
R_2, $\equiv \dfrac{\delta_2 U_G}{\nu}$, momentum-deficit Reynolds number;
s, $\equiv \dfrac{\tau}{\rho U_G^2}$, shear stress coefficient;
U_i, time-mean velocity in direction i;
U_τ, $\equiv \left(\dfrac{\tau_S}{\rho}\right)^{\frac{1}{2}}$, shear velocity;
U_G, time-mean velocity in free stream;
u_i, instantaneous fluctuating component of U_i;
x_i, cartesian coordinate system ($i = 1, 2, 3$), with streamwise direction in 1.

Greek symbols

σ_e, constant;
σ_1, σ_2, constants;
ρ, density of fluid;
ν, kinematic viscosity of fluid;
κ, constant;
η, $\equiv \dfrac{x_2}{[x_2]_G}$, non-dimensional distance from the wall;
λ, constant;
ε, $\equiv \dfrac{[x_2]_G}{2\rho C_D^{\frac{1}{2}}} \cdot \dfrac{dP}{dx}$;
τ, $\equiv \rho\left(\nu \dfrac{\partial U_1}{\partial x_2} - \overline{u_1 u_2}\right)$, total shear stress;
δ_1, $\equiv \displaystyle\int_0^\infty \left(1 - \frac{U_1}{U_G}\right) dx_2$, displacement thickness;
δ_2, $\equiv \displaystyle\int_0^\infty \frac{U_1}{U_G}\left(1 - \frac{U_1}{U_G}\right) dx_2$, momentum-deficit thickness;
θ, $\equiv [U_G^2 \cdot R_2]_0^{-1}$.

Subscripts

C, a point at the edge of the Couette flow;
G, the point where the boundary layer merges with the free stream;
S, a point at the wall;
0, starting station of the experiment.

1. INTRODUCTION

1.1. *Heat transfer and the turbulent boundary layer*

CONVECTIVE heat and mass transfer are processes which are dominated by hydrodynamics. It is therefore understandable that interest in heat transfer has been the motive for many investigations of a purely hydrodynamic character; for one must be able to predict the distributions of velocity and effective viscosity before there can be any hope of predicting temperature and convective heat flux; and, when the temperature differences are large enough to cause property variations, *simultaneous* solution of the hydrodynamic and heat-transfer problems is needed.

Motives of this kind have prompted two distinct lines of work: (i) development of numerical solution procedures; and (ii) the invention of turbulence models, i.e. sets of equations of which the solutions emulate, in important respects, real turbulent fluids. However, the mere existence of solution procedures and of turbulence models is not enough: it is necessary to determine, by careful comparison with experiment, whether their implications are indeed sufficiently realistic.

The present paper is a contribution to this validation process. It describes the application of an established solution procedure, combined with a recently-developed turbulence model, to sets of experimental conditions which have been subjected to scrutiny also by other workers. The general conclusion is that the procedure works well, and is therefore a satisfactory basis for use and further development.

1.2. *The equations of the hydrodynamic boundary layer*

It has long been established that, in a uniform-property two-dimensional, steady, turbulent boundary layer, having negligible normal turbulent stresses, the mean velocities are given by the following equations:

$$\frac{\partial U_1}{\partial x_1}+\frac{\partial U_2}{\partial x_2}=0, \tag{1.1}$$

and

$$U_1\frac{\partial U_1}{\partial x_2}+U_2\frac{\partial U_1}{\partial x_2}=\frac{\partial}{\partial x_2}\left(\nu\frac{\partial U_1}{\partial x_2}-\overline{u_1u_2}\right)-\frac{1}{\rho}\frac{\mathrm{d}P}{\mathrm{d}x_1}, \tag{1.2}$$

where $x_i (i = 1, 2, 3) \equiv$ cartesian coordinate system with direction 1 as that of the main stream,

$U_i \equiv$ time-mean velocity in the direction i,

$u_i \equiv$ instantaneous fluctuating component of U_i,

$P \equiv$ mean pressure in free stream,

$\nu \equiv$ kinematic viscosity of fluid,

and $\rho \equiv$ density of fluid.

In these equations, in addition to U_1 and U_2, the second-order correlation $\overline{u_1u_2}$ is another dependent variable; therefore, in order to solve the equation, additional information is required concerning the behaviour of $\overline{u_1u_2}$ in a boundary layer. Together with equations (1.1) and 1.2), and the boundary conditions, this information must completely specify the mathematical problem. Such information constitutes a "turbulence model".

In an earlier paper, Ng and Spalding [1] reported the development of a turbulence model based on the combined ideas of Prandtl [2] Kolmogorov [3] and Rotta [4]; the model specifies $-\overline{u_1u_2}$ as a product of the square root of the turbulent kinetic energy of the fluid e, $(\equiv \frac{1}{2}\{\overline{u_1^2}+\overline{u_2^2}+\overline{u_3^2}\})$, its length-scale of turbulence l, and the local mean velocity gradient. Both e and l are calculated from transport equations; the dependent variables of these are e and el. The model was shown in [1] to give realistic predictions for a number of self-similar boundary layers near walls. In the present paper, the model is applied to predict two-dimensional turbulent boundary-layer flows along smooth walls, subjected to non-uniform streamwise pressure gradients: the predictions are compared with experimental data, in order to draw some further conclusions on the degree of universality which the model possesses.

A brief description of the assumptions of the turbulence model will be given in Section 2; there is no change, even of numerical constants, from that which was reported in [1]. The method of solution and the boundary conditions for the relevant equations are described in Section 3; while the results of the predictions are presented in Section 4. Discussions of the predicted results, and their comparison with experiment, will be found in Section 5; this section also provides a comparison with predictions based upon a version of the mixing-length model of turbulence.

2. THE TURBULENCE MODEL

The essential features of the assumptions about the turbulent shear stress, energy and length scale are conveyed by the following equations:

(i) the effective-viscosity assumption:

$$-\overline{u_1u_2}=e^{\frac{1}{2}}l\frac{\partial U_1}{\partial x_2}; \tag{2.1}$$

(ii) the energy-conservation equation:

$$\underbrace{U_1\frac{\partial e}{\partial x_1}+U_2\frac{\partial e}{\partial x_2}}_{\text{convection}}=\underbrace{\frac{1}{\sigma_e}\frac{\partial}{\partial x_2}\left(e^{\frac{1}{2}}l\frac{\partial e}{\partial x_2}\right)}_{\text{diffusion}}+\underbrace{e^{\frac{1}{2}}l\left(\frac{\partial U_1}{\partial x_2}\right)^2}_{\text{generation}}-\underbrace{C_De^{\frac{3}{2}}/l}_{\text{dissipation}}; \tag{2.2}$$

(iii) the equation for the energy-length product:

$$\underbrace{U_1\frac{\partial el}{\partial x_1}+U_2\frac{\partial el}{\partial x_2}}_{\text{convection}}=\underbrace{\frac{\partial}{\partial x_2}\left(\frac{e^{\frac{1}{2}}l}{\sigma_1}\frac{\partial l}{\partial x_2}+\frac{e^{\frac{1}{2}}l^2}{\sigma_2}\frac{\partial e}{\partial x_2}\right)}_{\text{diffusion}}+\underbrace{C_Pe^{\frac{1}{2}}l^2\left(\frac{\partial U_1}{\partial x_2}\right)^2}_{\text{creation}}-\underbrace{C_Me^{\frac{3}{2}}}_{\text{destruction}}-\underbrace{C_W\left(\frac{l}{x_2}\right)^q e^{\frac{3}{2}}}_{\text{additional influence of the wall}}. \tag{2.3}$$

In these equations, x_2 represents the distance from the wall and the quantities, σ_e, C_D, σ_1, σ_2, C_P, C_M, C_W and q are assumed to be universal constants, the values of which are tabulated in Table 1. The origin of these values is described in [1], where it is shown that they give the best predictions for four cases of self-similar boundary-layer flows.

Table 1. The values of the constants in equations (2.2) and (2.3)

Constants	C_D	C_P	C_M	C_W	σ_e	σ_1	σ_2	q
Value	0.1	0.84	0.055	2.2	2	1.2	2	4

Equations (2.2) and (2.3) are valid under the conditions that: (i) the density of the fluid is uniform; and (ii) the Reynolds number of turbulence $e^{\frac{1}{2}}l/\nu$ is everywhere much greater than unity.

There will be no further discussion of the significance or validity of the various terms in equations (2.1), (2.2) and (2.3). However, it should be mentioned that, when the last term on the R.H.S. of equation (2.3) is neglected, the present model becomes identical to the one investigated by Rodi and Spalding [5] for jet flows *remote* from walls. The last term in equation (2.3) represents the additional influence of a solid boundary layer on the turbulence structure in a boundary layer; it vanishes for flows remote from walls, for which x_2 is very large.

3. SOLUTION PROCEDURE

The set of simultaneous equations (1.1), (1.2), (2.1), (2.2) and (2.3) can now be solved numerically for the dependent variables U_1, e and l. The solution procedure employed is the finite-difference method of Patankar and Spalding [6], which integrates the equations in a forward-marching procedure. However, to integrate those equations, one must prescribe suitable boundary conditions for the dependent variables; these boundary conditions can be classified into two types:

(i) *Boundary conditions at the edges of the boundary layer*

In a turbulent boundary layer on a wall, the flow can be divided into two regions: *a* and *b*, as shown in Fig. 1.

Region *b* is close enough to the wall for the convection terms of the differential equations to be negligible; it can be treated, for the purpose of calculating the velocity profile, as one-dimensional, i.e. a Couette flow. In the larger region, *a*, we can assume that $e^{\frac{1}{2}}l/\nu$ is much greater than unity; one consequence is that the first term within the parenthesis on the R.H.S. of equation (1.2) can be neglected.

Conditions within region b. The properties of the flow in region *b* can be deduced from well-known empirical functions, once the properties of flow at the point *C* (Fig. 1) are known. These empirical functions are:

$$\frac{[U_1]_C}{U_\tau} = \frac{1}{\kappa}\ln\left(E\cdot\frac{[x_2]_C U_\tau}{\nu}\right), \tag{2.4a}$$

$$[-\overline{u_1u_2}/e]_C = C_D^{\frac{1}{2}}, \tag{2.4b}$$

and

$$[l/x_2]_C = \kappa C_D^{\frac{1}{2}}, \tag{2.4c}$$

where $U_\tau \equiv (\tau_S/\rho)^{\frac{1}{2}}$, "shear-stress velocity", and κ and E are assumed to be universal constants, namely 0.435 and 9.0. These values have been chosen by reference to experimental measurements of velocity profiles near walls; the κ value is rather higher than has been presumed by some authors, but Patankar and Spalding [6] and Ng *et al.* [7] have had some success with it.

Equation (2.4a) is the well-established "law of the wall"; equations (2.4b) and (2.4c) express the results of measurements of the turbulence energy near walls [1]. It should be noted that both equations (2.4b) and (2.4c) satisfy equations (2.2) and (2.3) exactly in the one-dimensional region if the pressure gradient, dP/dx_1, vanishes; they are good approximate solutions even when dP/dx_1 is finite.

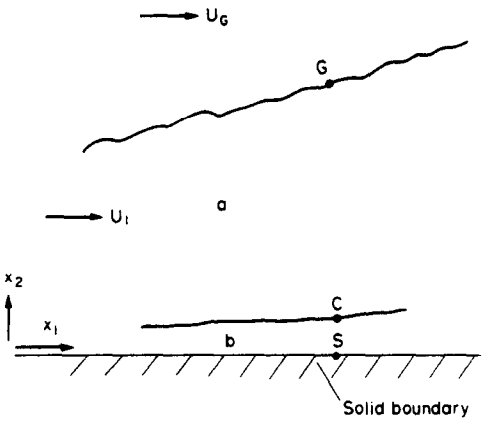

FIG. 1. The two regions (*a* and *b*) within a wall boundary layer.

The above relations can serve as boundary conditions for the small-x_2 edge of the domain of integration; this can therefore be confined to the region marked *a*.

(ii) *Boundary conditions at the free stream*

At the free-stream edge of the boundary layer, the following boundary conditions for the dependent variables are prescribed:

$$U_1 = U_G, \tag{2.5a}$$

$$e = 0, \tag{2.5b}$$

and

$$el = 0, \tag{2.5c}$$

where $U_G(x_1)$* ≡ the mean velocity of the main stream. Of course, one could also work with finite values of e and el, corresponding to a finite value of the free-stream turbulence; however, the turbulence levels in the streams of the experiments to be considered were not reported; but they were probably small.

(iii) *Initial profiles of* U_1, e *and* l

In addition to the boundary conditions discussed in the foregoing paragraph, one requires profiles of U_1, e and l at the upstream end of the forward integration. Of these three quantities, U_1 and e are directly measurable in a boundary layer. The profile of l can be deduced from equation (2.1) if, in addition to U_1 and e, the $\overline{u_1u_2}$ profile is known. When information concerning the initial profiles is absent, guesses must be made; those described in the Appendix have formed the bases of the computation to be presented; but the downstream results show little sensitivity to the starting condition in most cases.

(iv) *Some details of the numerical computations*

The results of predictions presented in the following section were obtained with 30 cross-stream grid points; the condition was imposed that $U_\tau[x_2]_C/\nu$ should be between 30 and 200; in general, grid points spaced to give equal amounts of mean flow between them were

*( ) means "a function of".

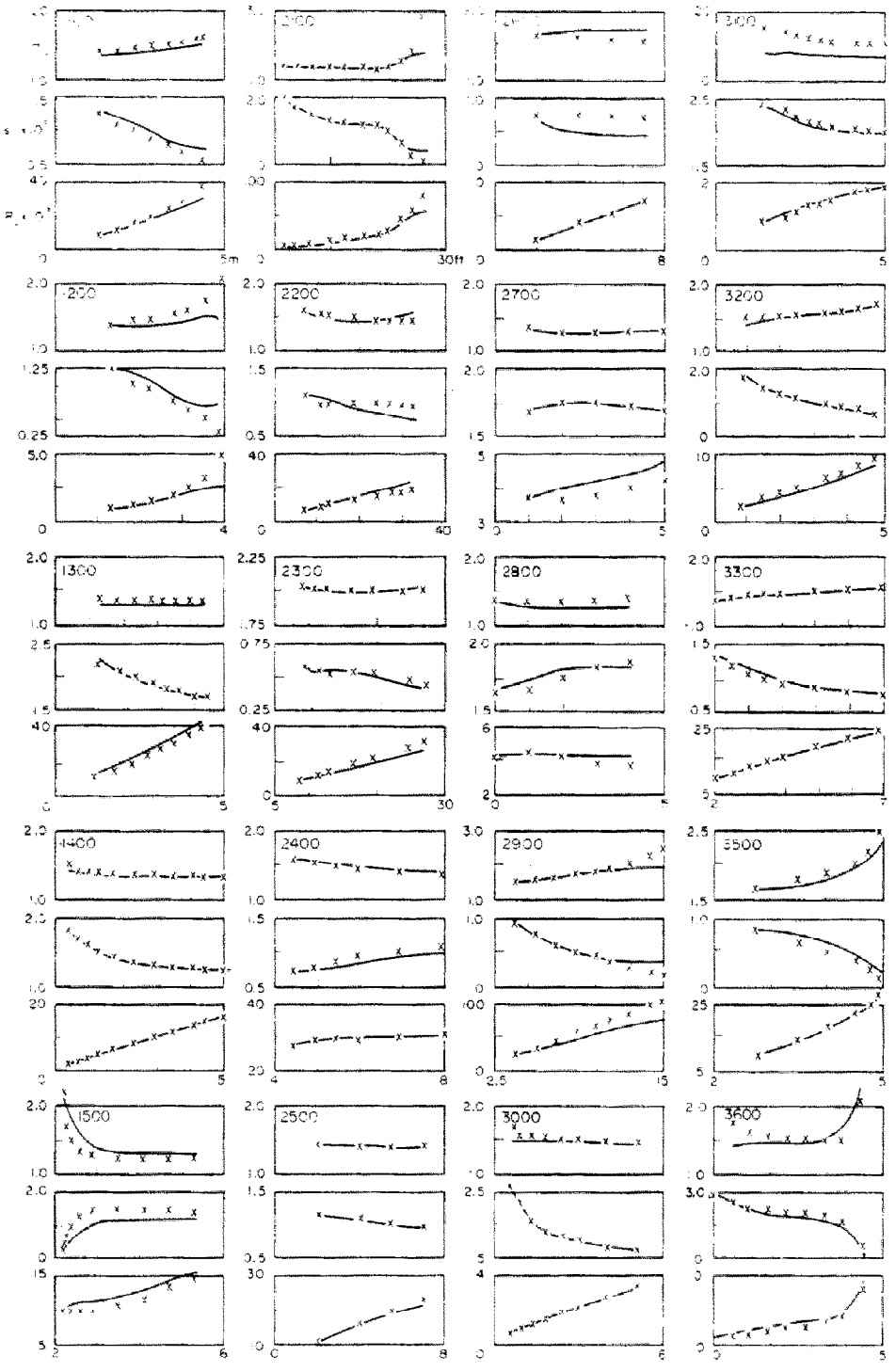

FIG. 2. (Continued on p. 1165.)

satisfactory in this respect. Computations made with other numbers and distributions of grids confirm that the above values give good computational accuracy.

The momentum balance of all the numerical solutions was also checked. In particular, the solution of a flat-plate boundary layer [8] showed that the rate of change of momentum-deficit thickness, $d\delta_2/dx_1$, is within 0.1% of its predicted local wall-shear coefficient s_S.

4. EXPERIMENTAL DATA CHOSEN FOR COMPARISON WITH PREDICTIONS

The differential equations have been solved with boundary conditions appropriate to the turbulent boundary-layer flow near walls which appear in the data collection of Coles and Hirst [9]. The information supplied is the $U_G \sim x_1$ variation and the starting profile of U_1. Unfortunately, the e and $-\overline{u_1 u_2}$ profiles are not provided for all the flows; so, in the predictions,

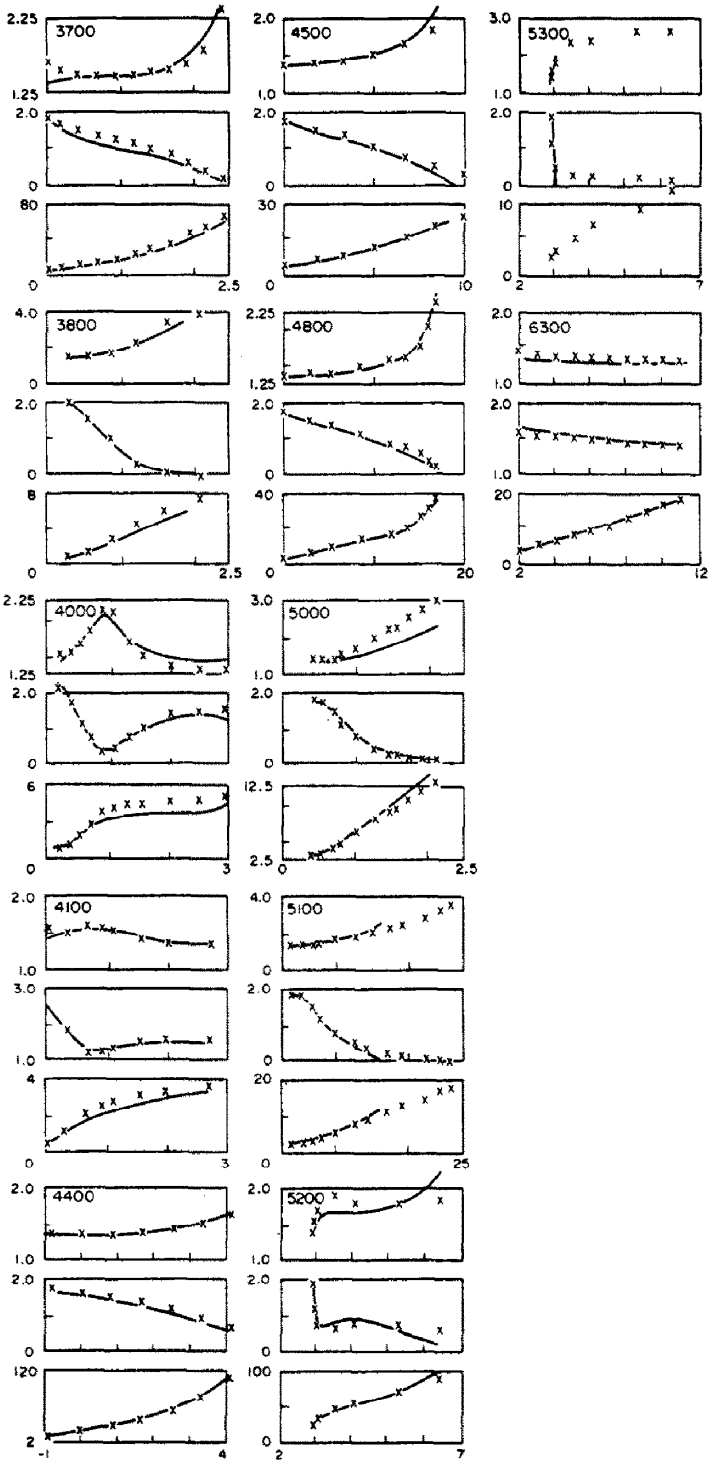

FIG. 2. Comparison of H_{12}, S_S and R_2 predictions with experiments; ——, prediction; ×, data according to [9].

it is assumed that e and l vary according to equations (A.1) and (A.2) at the starting point of the integration.

Results of predictions

In Fig. 2 are presented comparisons with all the experimental data apart from those for Riabouchinsky's moving-belt flow [10]. Each flow in the diagram is denoted by an identity number (IDENT); the nature of the experiment and the names of investigator(s) can be obtained from Table 2. For each flow, the predicted variation with x_1 of H_{12} ($\equiv \delta_1/\delta_2$, the shape factor), s_S ($\equiv \tau_S/\{\rho U_G^2\}$, the wall-shear coefficient) and R_2 ($\equiv \delta_2 U_G/\nu$, the momentum-deficit Reynolds number), is compared with the relevant experimental data; the lines represent predictions, and crosses represent data.

To facilitate more detailed inspection and discussion, six cases (IDENT = 1400, 2400, 2500, 2800, 3300 and 4800 in Fig. 2) are replotted to a larger scale in Figs.

Table 2. Name of investigator/s and nature of the experiment for flows shown in Fig. 2

IDENT	Investigator/s	Nature of experiment	Year
1100	Ludwieg and Tillmann	Mild adverse pressure gradient	1949
1200	Ludwieg and Tillmann	Strong adverse pressure gradient	1949
1300	Ludwieg and Tillmann	Accelerating flow	1949
1400	Wieghardt and Tillmann	Flat plate flow	1944
1500	Tillmann	Ledge flow	1945
2100	Schubauer and Klebanoff		1950
2200	Clauser	Flow No. 1	1954
2300	Clauser	Flow No. 2	1954
2400	Bradshaw and Ferriss	Relaxing flow	1965
2500	Bradshaw	$\alpha = -0.15$	1966
2600	Bradshaw and Ferriss	$\alpha = -0.255$	1965
2700	Herring and Norbury	$\beta = -0.35$	1967
2800	Herring and Norbury	$\beta = -0.53$	1967
2900	Perry		1966
3000	Bell	Constant pressure	1966
3100	Bell	Series D	1966
3200	Bell	Series E	1966
3300	Bradshaw	$\alpha = 0 \rightarrow -0.255$, C	1967
3500	Newman	Airfoil, Series 2	1951
3600	Moses	Case 1	1964
3700	Moses	Case 2	1964
3800	Moses	Case 3	1964
4000	Moses	Case 5	1964
4100	Moses	Case 6	1964
4400	Schubauer and Spangenberg	Flow A	1960
4500	Schubauer and Spangenberg	Flow B	1960
4800	Schubauer and Spangenberg	Flow E	1960
5000	Fraser	Flow A	1956
5100	Fraser	Flow B	1956
5200	Stratford	Experiment 5	1959
5300	Stratford	Experiment 6	1959
6300	Bauer	Spillway, 60°	1951

3–8. For the first five of these, the predictions of U_1, τ and e are also compared with the available data at the last station of the relevant experiment; these predictions and data are displayed in Figs. 9–13.

5. DISCUSSION

5.1. *Comparison of the predictions with experiments*

From Fig. 2, one can infer that the predictions agree tolerably with the experimental data. Inspection of all predictions made by other methods for the same conditions, reported in the Proceedings of the Stanford Conference, shows that where the present method fails, e.g. IDENT = 1200, 2900 and 5300, most of the other methods fail also; there is reason to suppose that these flows were not truly two-dimensional. The present predictions appear to be in as good agreement with the data as the experimental accuracy warrants.

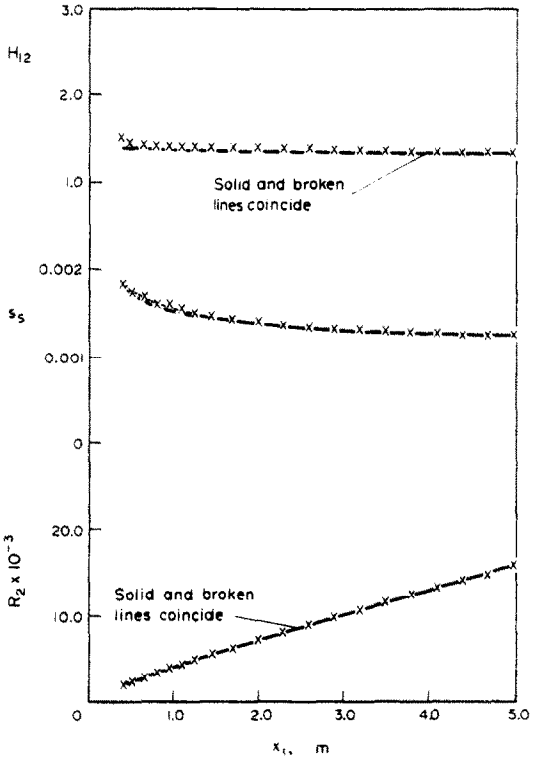

FIG. 3. Comparison of prediction of H_{12}, S_S and R_2 with the experimental data of Wieghardt and Tillmanns' flat plate flow [8] (IDENT = 1400); ——, present prediction; – – –, mixing-length model; ×, data.

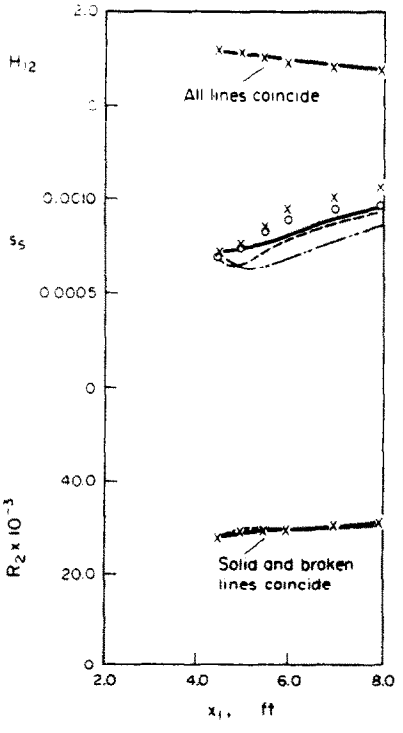

FIG. 4. Comparison of prediction of H_{12}, S_S and R_2 with the experiment of Bradshaw and Ferriss [17] (IDENT = 2400); ——, present model with the initial profile of e from equation (A.1) or with e and l profiles from the experiment; –·–, present model with initial profile of e from equation (5.1); – – – –, mixing-length model; ×, data according to Coles and Hirst; ○, data according to [17].

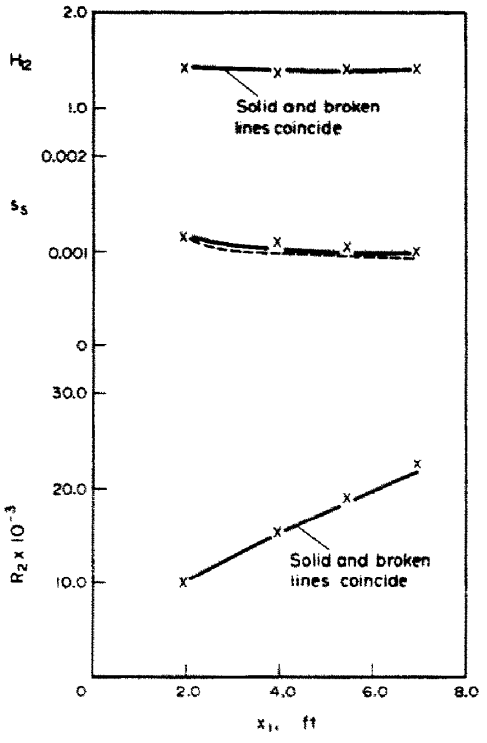

FIG. 5. Comparison of prediction of H_{12}, S_S and R_2 with the experiment of Bradshaw [20] "$\alpha = -0.15$" (IDENT = 2500); ——, present model with initial profile of e from equation (A.1) or equation (5.1) or with initial profiles of e and l from the experiment; – – – –, mixing-length model; ×, data.

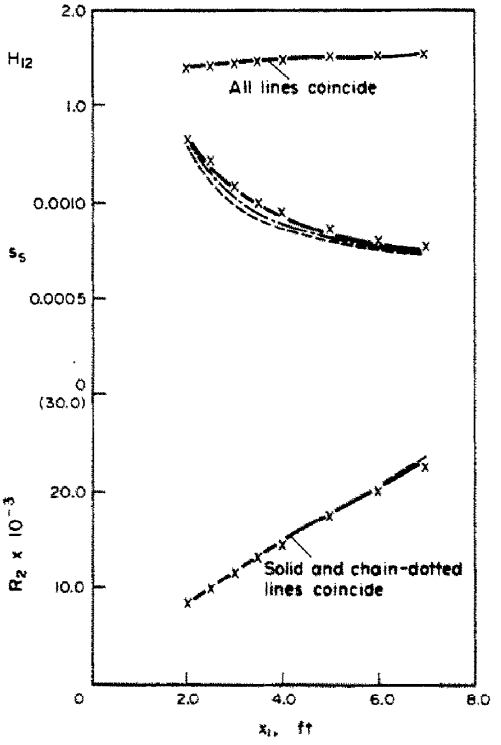

FIG. 7. Comparison of prediction of H_{12}, S_S and R_2 with the experiment of Bradshaw [20] "$\alpha = 0 \rightarrow -0.255$, Flow C" (IDENT = 3300); ——, present model; –·–, present model with initial profiles of e and l from the experiment; – – – –, mixing-length model; ×, data.

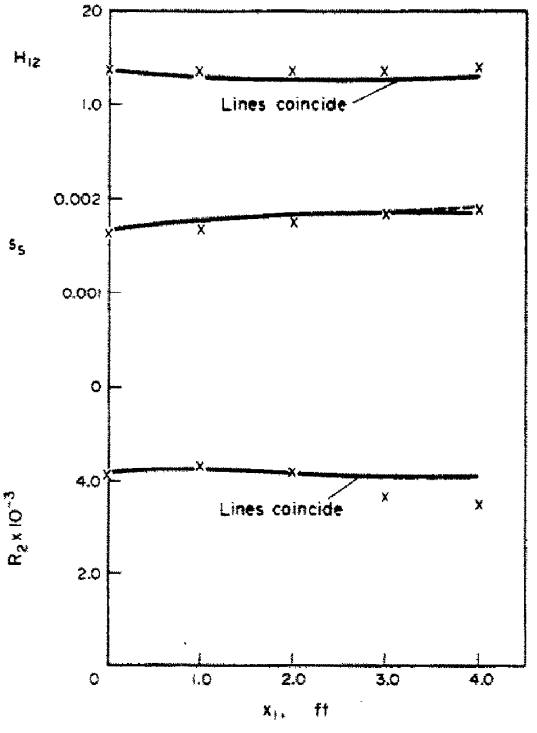

FIG. 6. Comparison of prediction of H_{12}, S_S and R_2 with the experiment of Herring and Norbury [19]. "$\beta = -0.53$" (IDENT = 2800); ——, present model with initial e profile from equation (A.1) or (5.1); – – – –, mixing-length model; ×, data.

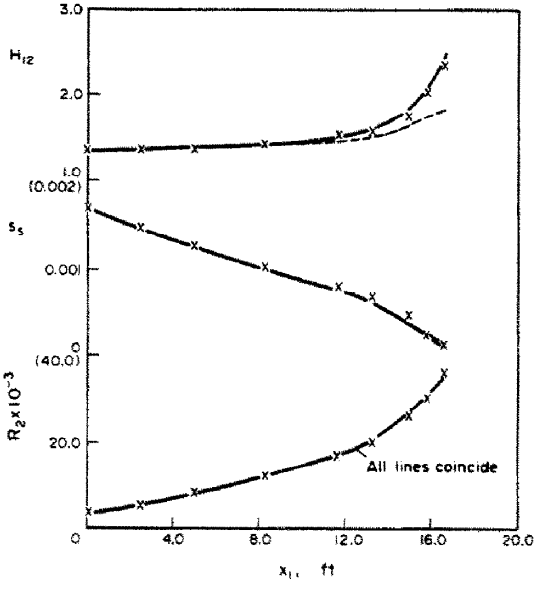

FIG. 8. Comparison of prediction of H_{12}, and R_2 with the experiment of Schubauer and Spangenberg [27] "Flow E" (IDENT = 4800); ——, present model; – – – –, mixing-length model; ×, data.

Possible sources of error in the predictions. (a) *The "log-law" assumption (equation 2.4a) close to the wall*— The present prediction method employs the logarithmic law of the wall, for the calculation of τ_S from U_1 and x_2 at the point C (see Fig. 1). This practice is relatively

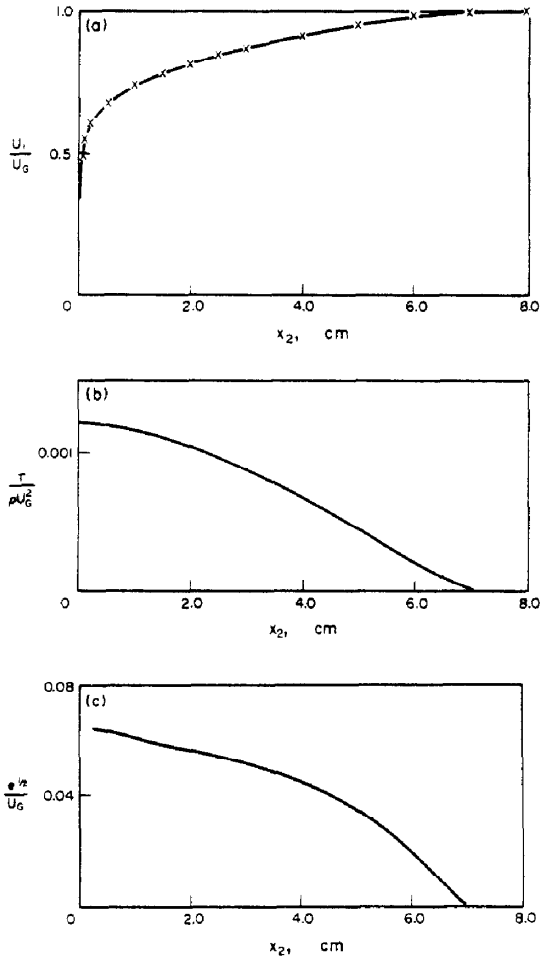

FIG. 9. Comparison of predicted U_1, τ and e profiles with the experiment of Wieghardt and Tillmann [8] at $x_1 = 4.987$ m; ——, prediction; ×, data. (a) Comparison of the U_1/U_G profile. (b) Predicted $\tau/(\rho U_G^2)$ profile; data not available. (c) Predicted $e^{\frac{1}{2}}/U_G$ profile; data not available.

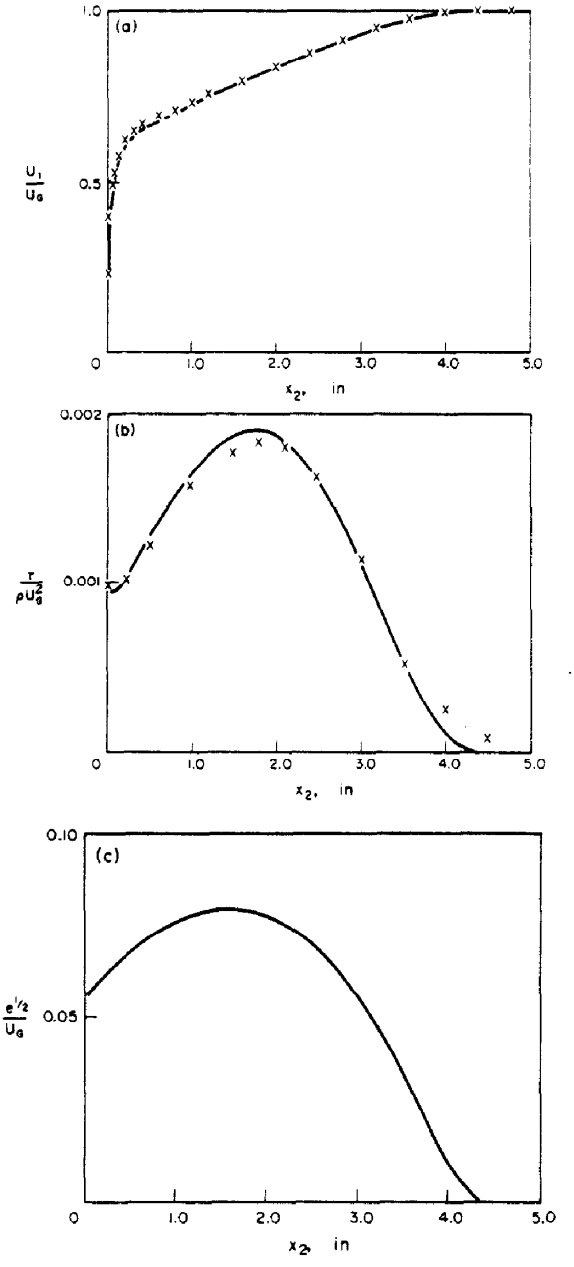

FIG. 10. Comparison of predicted U_1, τ and e profiles with the experiment of Bradshaw and Ferriss at $x_1 = 7.9$ ft; ——, prediction; ×, data. (a) Comparison of the U_1/U_G profile. (b) Comparison of the $\tau/(\rho U_G^2)$ profile. (c) Predicted $e^{\frac{1}{2}}/U_G$ profile; data not available.

simple, and in reasonable agreement with experimental data over a wide range of flow conditions. In reality however, τ_S must depend upon other variables, such as dP/dx_1 and $[e]_C$ etc. The effect of the former has been accounted for in the "wall-law" developed by Patankar and Spalding [6]; and the latter influence appears in formulae developed by Spalding [11] Wolfshtein [12] and Runchal [13]. It will be valuable to establish later, whether any of these proposals can improve agreement with reliable experimental data.

(b) *The assumption concerning the starting profiles*—It may be recalled that, for all the predictions shown in Fig. 2, the initial profiles of e and l have had to be based on the procedure in the Appendix. In order to test the influence of the starting profiles, flows 2400, 2500 and 3300 were recalculated with initial profiles of e and l identical to those which, in these cases, were reported by the experimenters [l is deduced from τ, e and U_1 profiles according to equation (2.1)]. Wherever these predictions deviate from the earlier result, they are represented by chain-dotted (–·–) lines in Figs. 4, 5 and 7; they show little difference from the earlier predictions, indicating that the assumed profiles for e and l [equations (A.1) and (A.2)] are adequate for these flows.

As a further test, flows 2400, 2500 and 2800 were repeated with a linear initial profile of e, namely:

$$e = a(1-\eta), \tag{5.1}$$

where

$$\eta \equiv x_2/[x_2]_G.$$

This profile would be realistic had the flow not been subjected to any pressure variation upstream of the starting point. The predictions are shown in double-chained (–··–) lines in Figs. 4–6. For flows 2500 and 2800 (Figs. 5 and 6), there are no discernible differences

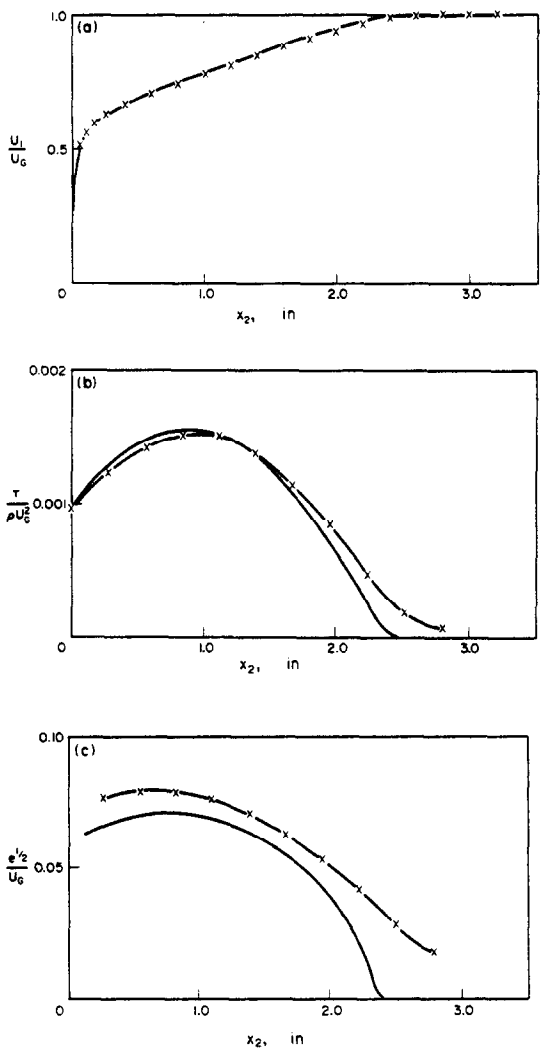

FIG. 11. Comparison of predicted U_1, τ and e profiles with the experiment of Bradshaw "$\alpha = 0.15$" at $x_1 = 7$ ft. (a) Comparison of the U_1/U_G profile; ——, prediction; ×, data. (b) Comparison of the $\tau/(\rho U_G^2)$ profile; ——, prediction; - × -, data. (c) Comparison of the $e^{\frac{1}{2}}/U_G$ profile; ——, prediction; - × -, data.

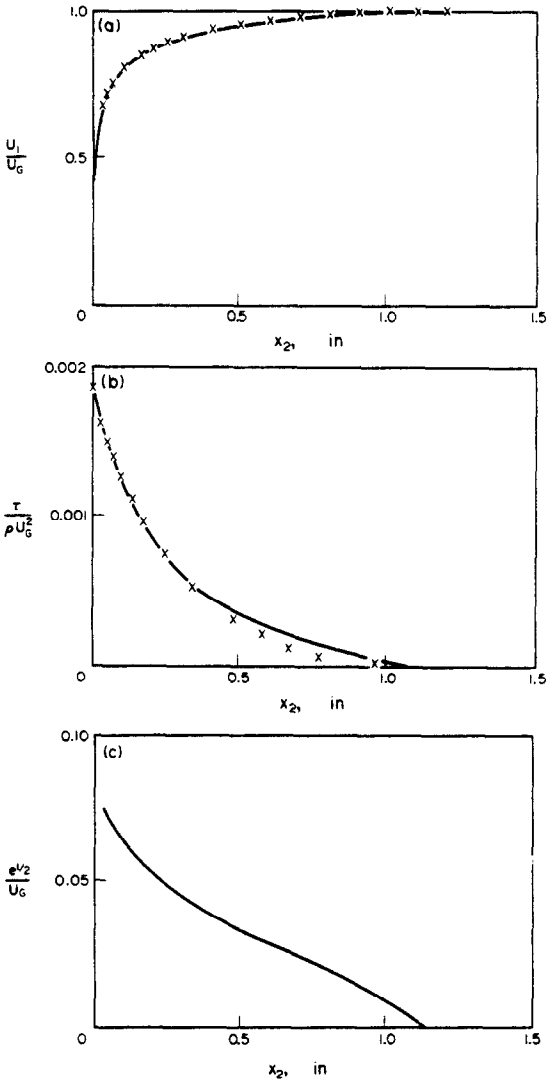

FIG. 12. Comparison of predicted U_1, τ and e profiles with the experiment of Herring and Norbury "$\beta = -0.53$" at $x_1 = 4$ ft; ——, prediction; ×, data. (a) Comparison of the U_1/U_G profile. (b) Comparison of the $\tau/(\rho U_G^2)$ profile. (c) Predicted $e^{\frac{1}{2}}/U_G$ profile; data not available.

between the predictions with the two different starting profiles; the solid and double-chained lines coincide. However, for flow 2400, although there is no significant difference in the prediction of R_2 and H_{12}, a worse prediction of s_S is obtained as shown in Fig. 4. This is explainable by the fact that, downstream of a severely decelerated flow, the e profile would be closer to equation (A.1) than to equation (5.1). In most boundary layers, the e profile should lie between these two, depending on its upstream conditions.

Factors affecting the accuracy of the experimental data. (a) *Data for the wall-shear coefficient*, s_S—The "experimental" values of s_S are based not on direct measurements, but on deductions from velocity-profile measurements by the "Clauser-plot" method; this employs equation (2.4a) but with κ as 0.41 and E as 7.8. Some indication of the accuracy of the data for s_S can be obtained from Fig. 4. In the figure, the differences are displayed of the values deduced by Coles and Hirst by the Clauser-plot method from those deduced by Bradshaw and Ferriss from Preston-tube measurements for the same experimental conditions. Differences as large as 10% can be seen.

(b) *The lateral convergence or divergence of the boundary layer*—In wind-tunnel measurements, boundary-layer growth along the side walls can cause lateral convergence or divergence of the boundary layer under investigation; then equations (1.1), (1.2), (2.2) and (2.3) cease to be valid. This breakdown is evident in flow 2100 (Fig. 2). Figure 14 shows the same effect by way of the quantities PL and PR, the definitions of which are displayed in the figure. In a boundary-layer flow without convergence, PL should be equal to PR. However, as shown in the figure, PL starts to deviate from PR at x_1 of about 23 ft. Insofar as this is not due to incorrect values of s_S or to the breakdown of other

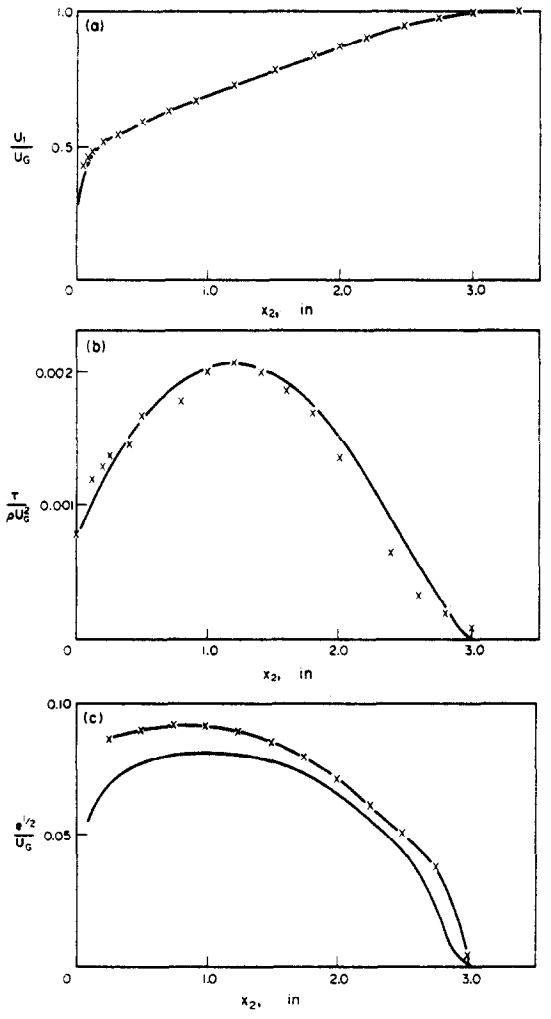

FIG. 13. Comparison of predicted profiles of U_1, τ and e with the experiment of Bradshaw "$\alpha = 0 \rightarrow -0.255$, Flow C" at $x_1 = 7$ ft. (a) Comparison of the U_1/U_G profile; ——, prediction; ×, data. (b) Comparison of the $\tau/(\rho U_G^2)$ profile; ——, prediction; ×, data. (c) Comparison of the $e^{\frac{1}{2}}/U_G$ profile; ——, prediction; – × –, data.

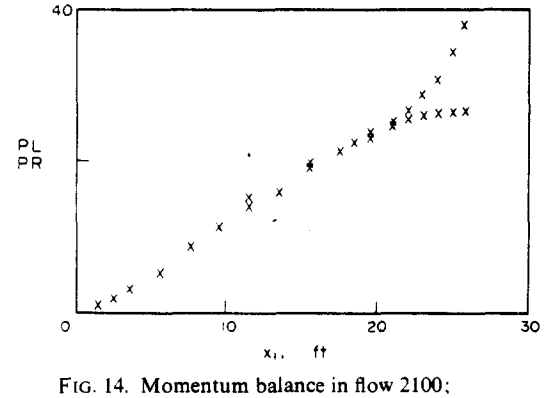

FIG. 14. Momentum balance in flow 2100;

$$PL \equiv \theta(U_G^2 R_2) - 1 + \theta \int_{[x_1]_0}^{x_1} H_{12} R_2 U_G \, dU_G$$

$$PR \equiv \theta \int_{[x_1]_0}^{x_1} U_T^2 \nu^{-1} \, dx_1$$

where $[x_1]_0$ is defined as the starting point of the experiment and θ as $1/[U_G^2 R_2]_0$; ×, PL, Δ, PR.

boundary-layer assumptions, the cause can be attributed to the lateral convergence of the boundary layer. As indicated in Fig. 2, the predictions start to deviate from the experimental data at about the same position as PL deviates from PR.

(c) *Inadequate number of points to specify the mean-velocity profile*—The integral parameters H_{12} and R can be wrongly ascribed when there are too few cross-stream points close to the wall to allow correct determination of the velocity profile. This is probably the cause of disagreement in H_{12} between experiment and prediction of flows 3100, 3600, 3700 and 4100 in Fig. 2.

Comparison of predicted U_1, e *and* τ *profiles with experiments*

Figures 9–13 display the predicted profiles of U_1/U_G, $\tau/(\rho U_G^2)$ and $e^{\frac{1}{2}}/U_G$ at the last station of flows 1400, 2400, 2500, 2800 and 3300, and compare them with the available data. The mean-velocity profiles are well predicted for all five cases. However, as shown in Fig. 11, the predicted boundary-layer thickness appears to be smaller than that of the experimental data. Since the model no longer requires the boundary-layer thickness to determine the length scale as do the models employed by Glushko [14], Patankar and Spalding [6], Bradshaw *et al.* [15] and Nee and Kovasznay [16], the slight discrepancy in the predicted boundary-layer thickness should not seriously affect the correct prediction of other properties of the flow.

A more rigorous test of the turbulence model is its ability to predict the τ profiles correctly. The comparisons of these profiles with data are shown in Figs. 10b, 11b, 12b and 13b. It is noted that for all cases, the τ profile has not been well predicted near the free-stream edge of the boundary layer, where however, the value of τ is small compared with its local maximum.

The predicted profiles for $e^{\frac{1}{2}}/U_G$ seem to fall below the experimental values as shown in Figs. 11c and 13c. This perhaps is due to the fact that the value of C_D, taken as 0.1, is somewhat too large. According to [1], the data for pipe flows indicate that C_D varies between 0.06 and 0.09. The best value of C_D can be determined only by further research.

Near the free stream (Figs. 11c and 13c), the discrepancy between predicted and measured e's may be further increased by the presence of free-stream turbulence in the experiments; free-stream turbulence has been left out of the present predictions [see equation (2.5b)], although it would be easy to include it if data on its magnitude were available.

5.2. *Comparisons of predictions using the present model with those using the mixing-length model*

The results of prediction by Prandtl's mixing-length model for flows 1400, 2400, 2500, 2800, 3300 and 4800 (see Ng *et al.* [7]) are displayed in Figs. 3–8 in dotted lines.

For flows 1400, 2500, 2800 and 3300, there is no great difference in the predictions between the present model and the mixing-length model as shown in Figs. 3 and 5–7. However, for strongly non-equilibrium flows, like

2400 and the downstream part of 4800, the present model gives better predictions of the overall properties of the boundary layer.

5.3. *Use of the model for the prediction of heat transfer*

Now that the computational procedure has been shown to be adequate for the prediction of the hydrodynamics of two-dimensional turbulent boundary layers, its extension to heat-transfer is straightforward. Several ways of making the extension are possible, namely:

(a) By way of an "analogy", for example, that of Chilton and Colburn [21].

(b) By use of a more sophisticated connection between the shear-stress distribution and the heat-transfer rate, for example, that of Spalding [22], as extended by Kestin and Persen [23], Gardner and Kestin [24], Smith and Shah [25] and Spalding [26].

(c) By solution of an additional partial differential equation, namely that for stagnation enthalpy, as in the work of Patankar and Spalding [6].

Of method (a) it may be said that the method is simple but inaccurate, especially when gradients of stream velocity and of wall temperature are significant. It would be unreasonable, if heat-transfer predictions were the main desired outcome, to take so much trouble over the hydrodynamics and so little over the thermal effects.

Method (b) is somewhat more tedious to perform; but the work involved is less demanding than that associated with the solution of an additional differential equation. It may be the most accurate method for high Prandtl numbers, for which the thermal boundary layer is confined to the region very close to the wall.

For moderate or low Prandtl numbers, method (c) is to be preferred; and, since three differential equations are already being solved, the addition of a fourth is no great matter. Of course, an assumption must be made for the effective thermal conductivity of heat. At present, the only sufficiently-tested assumption is that which rests on the existence of an effective (turbulent) Prandtl number, the value of which is of the order of unity, and to be determined from experiments. This is the assumption incorporated into the computer program of [6].

6. CONCLUSIONS

(1) The present model of turbulence is capable of predicting steady two-dimensional, hydrodynamic, turbulent boundary layers on smooth walls with non-uniform streamwise pressure gradients, from one set of constants.

(2) The accuracy of prediction is as satisfactory as the reliability of the data warrants.

(3) The values of some of the constants in the model can probably still be adjusted to improve agreement between the prediction and the most reliable of the experimental data.

(4) For flows near the state of local equilibrium, there is no discernible difference between the predictions of the present model and those of the mixing-length model.

(5) The present model gives better predictions than the mixing-length model for non-equilibrium boundary layers when the experimental starting profiles are provided for U_1, e and τ.

(6) The model and calculation procedure therefore form a satisfactory basis on which to build a method of calculating convective heat transfer.

REFERENCES

1. K. H. Ng and D. B. Spalding, A turbulence model for boundary layers near walls, *Physics Fluids* **15**(1), 20–30 (1972).
2. L. Prandtl, Uber ein neues Formelsystem fur die ausgebildete Turbulenz, Nachr. Wiss. Göttingen. Van den Loeck and Ruprecht (1945).
3. A. N. Kolmogorov, Equation of turbulent motion of an incompressible fluid, *Izv. Akad. Nauk. S.S.S.R. ser. Phys.* 1–2 (1942).
4. J. C. Rotta, Statistiche Theorie nichtomogener Turbulenz, *Z. Phys.* **131**, 51 (1951).
5. W. Rodi and D. B. Spalding, A two-parameter model of turbulence and its application to free jets, *Wärme- und Stoffübertragung* **3**, 85 (1970).
6. S. V. Patankar and D. B. Spalding, *Heat and Mass Transfer in Boundary Layers*. Morgan-Grampian, West Wickham (1967).
7. K. H. Ng, S. V. Patankar and D. B. Spalding, in *Proceedings of the Conference on Computation of Turbulent Boundary Layers*—1, Edited by S. J. Kline, M. V. Morkovin, G. Sovran and D. J. Cockrell. Stanford University Press, Stanford (1968).
8. K. Wieghardt and W. Tillmann, On the turbulent friction layer for rising pressure, U. and M. 6617 (1944).
9. D. E. Coles and E. A. Hirst, Proceedings of the conference on computation of turbulent boundary layers—2. Stanford University Press, Stanford (1968).
10. D. Riabouchinsky, Etude experimentale sur le frottement de l'air, *Bull. Inst. Aerodyn. Koutchino* **5**, 51–72 (1914).
11. D. B. Spalding, Monograph on turbulent boundary layers, Chapter 2, I.C. Mech. Eng. Dept. Rep. TWF/TN/33 (1967).
12. M. Wolfshtein, The velocity and temperature in one-dimensional flow with turbulence augmentation and pressure gradient, *Int. J. Heat Mass Transfer* **12**, 301 (1969).
13. A. K. Runchal, Transfer processes in steady two-dimensional separated flows, Ph.D. Thesis, London University (1969).
14. G. S. Glushko, The turbulent boundary layer on a flat plate, *Izv. Akad. Nauk. SSSR, Mekh.* **4**, 13 (1965).
15. P. Bradshaw, D. H. Ferriss and N. P. Atwell, Calculation of boundary-layer development using the turbulent energy equation, *J. Fluid Mech.* **28**, 593 (1967).
16. V. W. Nee and L. S. Kovasznay, Simple phenomenological theory of turbulent shear flows, *Physics Fluids* **12**, 473 (1969).
17. P. Bradshaw and D. H. Ferriss, The response of a retarded equilibrium turbulent boundary layer to sudden removal of pressure gradient, NPL Aero. Rep. 1145 (1965).
18. P. Bradshaw, The turbulence structure of equilibrium boundary layers, *J. Fluid Mech.* **29**, 265 (1967).
19. H. Herring and J. Norbury, Some experiments on equilibrium turbulent boundary layers in favourable pressure gradients, *J. Fluid Mech.* **27**, 541 (1967).
20. P. Bradshaw, The response of a constant-pressure turbulent boundary layer to the sudden application of an adverse pressure gradient, ARC R and M 3575 (1967).
21. T. H. Chilton and A. P. Colburn, Mass transfer (absorption) coefficients. Prediction from data on heat transfer and fluid friction, *Ind. Engng Chem.* **26**, 1183–1187 (1934).

22. D. B. Spalding, Heat transfer to a turbulent stream from a surface with a step-wise discontinuity in wall temperature, in *International Developments in Heat Transfer*, Part II, pp. 439–446. A.S.M.E., New York (1961).
23. J. Kestin and L. N. Persen, Application of Schmidt's method to the calculation of Spalding's function and of the skin-friction coefficient in turbulent flow, *Int. J. Heat Mass Transfer* **5**, 143–152 (1962).
24. G. C. Gardner and J. Kestin, Calculation of the Spalding function over a range of Prandtl numbers, *Int. J. Heat Mass Transfer* **6**, 289–299 (1963).
25. A. G. Smith and V. L. Shah, The calculation of wall and fluid temperatures for the incompressible turbulent boundary layer, with arbitrary distribution of wall heat flux, *Int. J. Heat Mass Transfer* **5**, 1179–1189 (1962).
26. D. B. Spalding, A single formula for the law of the wall, *J. Appl. Mech.* **83E**, 455–458 (1961).
27. G. B. Schubauer and W. G. Spangenberg, Forced mixing in boundary layers, *J. Fluid Mech.* **8**, 10–32 (1960).

APPENDIX

The starting profile of e is assumed to be:

$$e = a + b\eta + c\eta^2 + d\eta^3. \tag{A.1}$$

In this equation, the quantities a, b, c and d are evaluated from the following conditions for e:

(i) at $\eta = [\eta]_C$,

$$e = C_D^{\frac{1}{2}}\left[\frac{\tau}{\rho}\right]_C$$

and $de/d\eta = \varepsilon + |\varepsilon|$,

where $\varepsilon \equiv \dfrac{[x_2]_G}{2\rho C_D^{\frac{1}{2}}} \cdot \dfrac{dP}{dx_1}$;

(ii) at $\eta = 1$,

$$e = 0,$$

and $de/d\eta = 0$.

(iii) For l, it is assumed that:

$$l = C_D^{\frac{1}{2}} l_m. \tag{A.2}$$

In this equation, l_m is the mixing length; thus,

$$l_m = \kappa x_2 \text{ for } \lambda/\kappa > \eta > 0$$

and

$$l_m = \lambda \cdot [x_2]_G \text{ for } 1 > \eta \geqslant \lambda/\kappa,$$

where $\lambda \equiv 0.09$, a constant.

PREVISION NUMERIQUE DE COUCHES LIMITES BIDIMENSIONNELLES SUR PAROIS LISSES A L'AIDE D'UN MODELE DE TURBULENCE A DEUX EQUATIONS

Résumé—La couche limite hydrodynamique turbulente bidimensionnelle stationnaire, incompressible près d'une paroi a été calculée à l'aide d'un modèle de turbulence. Ce dernier rattache la tension de cisaillement turbulent au produit des grandeurs suivantes: la racine carrée de l'énergie locale de turbulence, une échelle de turbulence et le gradient de vitesse moyenne. L'echelle de turbulence et l'énergie sont obtenues à partir d'équations aux dérivées partielles paraboliques résolues en simultanéité avec l'équation du mouvement. Des couches limites présentant diverses distributions longitudinales de pression, telles que celles décrites dans les travaux de la Conférence de Stanford (1968), ont été calculées avec succés. Des méthodes d'extension à la prévision du transfert de chaleur sont discutées.

ZUR BERECHNUNG ZWEIDIMENSIONALER GRENZSCHICHTEN AN GLATTEN WÄNDEN MIT EINEM ZWEIGLEICHUNGS-MODELL FÜR DIE TURBULENZ

Zusammenfassung—Es wurden zweidimensionale, stationäre, inkompressible, turbulente Strömungsgrenzschichten an Wänden berechnet. Dabei wurde ein Turbulenzmodell verwendet, bei dem die turbulente Schubspannung mit dem Produkt aus der Quadratwurzel der lokalen Energie der Turbulenz, einer kennzeichnenden Länge der Turbulenz und des Gradienten Zeit-mittlere Geschwindigkeit verknüpft wird. Sowohl die kennzeichnende Länge wie die Energie werden aus parabolischen Differentialgleichungen berechnet, die gleichzeitig mit der Differentialgleichung für den Impuls gelöst werden. Grenzschichten mit einer starken Änderung der Druckverteilung in Strömungsrichtung, nämlich solche, die auf der Stanford-Konferenz 1968 vorgestellt wurden, konnten erfolgreich berechnet werden. Methoden zur Ausdehnung des Verfahrens auf die Berechnung des Wärmeübergangs werden diskutiert.

РАСЧЕТ ДВУМЕРНЫХ ПОГРАНИЧНЫХ СЛОЕВ НА ГЛАДКИХ СТЕНКАХ С ПОМОЩЬЮ МОДЕЛИ ТУРБУЛЕНТНОСТИ, ОПИСЫВАЕМОЙ ДВУМЯ УРАВНЕНИЯМИ

Аннотация — Дан расчет двумерных стационарных несжимаемых турбулентных гидродинамических пристенных пограничных слоев с помощью модели турбулентности, связывающей турбулентное сдвиговое напряжение с произведением квадратного корня локальной энергии турбулентности на масштаб турбулентности и градиент средней по времени скорости. Масштаб и энергия определяются из параболических дифференциальных уравнений, решаемых одновременно с уравнениями количества движения. С успехом рассчитаны пограничные слои, характеризующиеся большим разнообразием распределений давления по течению, т. е. тех, о которых говорилось в 1968 г. на конференции в Стэнфорде. Обсуждается применение данного метода для расчета теплообмена.